DISCRETE AND CONTINUOUS
DYNAMICAL SYSTEMS SERIES S

doi:10.3934/dcdss.2022058

BACK-AND-FORTH NUDGING FOR THE QUASI-GEOSTROPHIC OCEAN DYNAMICS WITH ALTIMETRY: THEORETICAL CONVERGENCE STUDY AND NUMERICAL EXPERIMENTS WITH THE FUTURE SWOT OBSERVATIONS

Samira Amraoui, Didier Auroux* and Jacques Blum

Université Côte d'Azur, CNRS, LJAD, France

Emmanuel Cosme

Université Grenoble Alpes, CNRS, IRD, G-INP, IGE, France

Abstract. In data assimilation for geophysical problems, the increasing amount of satellite data to analyze makes it more and more challenging to guarantee near real time forecasting. Thus, low time and memory consuming data assimilation methods become very attractive. The back-and-forth nudging (BFN) method is a non-classical data assimilation method that can be seen as a deterministic and smoothing version of the Kalman filter. From a practical point of view, the BFN method is very valuable for its simplicity of implementation (no optimization, no differentiation,...) and its rapidity of convergence. Under observability conditions, we prove the mathematical convergence of BFN at deep layers for a multi-layer quasi-geostrophic (MQG) ocean circulation model using an infinite dimensional variant of LaSalle's invariance principle. We also extend the BFN to the problem of joint state-parameter identification. The numerical experiments, performed on 120km large swath sea surface height (SSH) simulated data of the Surface Water Ocean Topography (SWOT) satellite, show the high robustness of the algorithm to uncertainties and the few iterations needed to reach convergence, whereas some problems remain due to non-reversibility properties in time. We also give a strategy to improve geophysical model accuracy, considering the large number of uncertain parameters inherent to models and their impacts on state estimation performance. We propose here a joint state-parameter estimation, tested on the baroclinic wavenumber as an unobserved parameter.

1. **Introduction.** Reliable weather maps are necessary for many operational and climatological applications. For instance in weather forecasting a special effort is usually made to fully reconstruct the initial state, essential to start a forecast process. In practice information provided by measurements is too limited to define a complete field based only on collected data. Data assimilation techniques are used to solve this underdetermined inverse problem. The idea is to provide an estimation that is both close to the available observations and satisfying the dynamical

2020 *Mathematics Subject Classification.* Primary: 86A05, 86A22, 93D05; Secondary: 35Q86, 35R30, 37N10, 65M32, 93B53.

Key words and phrases. Oceanography, wide-swath altimetry, nudging-based data assimilation, parameter estimation, Lyapunov-based convergence.

This paper is dedicated to the memory of François-Xavier Le Dimet who left us in March 2021. He was an expert in data assimilation and at the origin of the 4D-VAR algorithm, especially in meteorology.

* Corresponding author: Didier Auroux.

evolution of the physical phenomenon. The nudging method is a data assimilation method historically used for meteorological problems [23, 38], also known as Luenberger observer in control theory [31]. It consists in adding, in some equations of the dynamical model, a relaxation term towards available observations. This term is supposed to draw the simulated state of the nudging system towards the real state of the observed system [10].

Another variant of the standard nudging method called *back-and-forth nudging* (BFN) was introduced by Auroux and Blum [6, 7]. The novelty of BFN is to use a backward nudged integration of the model, and multiple iterations of forward and backward model integrations until convergence. This allows the algorithm to converge on finite time windows, while the standard nudging (or asymptotic observer) usually requires a very long time window (theoretically, an infinite time) to converge. BFN is a simple method that does not require linearization, making it a valuable candidate for most nonlinear geophysical problems. The back-and-forth strategy has the advantage, over the classical time asymptotic data assimilation methods, of assimilating each data as many times as necessary to obtain a satisfactory estimation and most importantly of providing an accurate estimation of the initial condition. This drives us to explore theoretical and practical results of convergence for state reconstruction with the BFN method.

The convergence of BFN was widely studied for well-posed linear dynamical ODEs or PDEs, such as transport equation [9]. For ODE systems, the pole shifting theorem demonstrates that an asymptotically stable nudging model exists if the system is exactly observable. Donovan et al. [17] have proposed an explicit way to determine the corresponding nudging gain matrix. But for nonlinear problems, these techniques are hard to transpose and a careful examination on theoretical convergence of BFN is still required. To our knowledge, few work has been undertaken to prove the BFN convergence for nonlinear problems; we can mention the work of Auroux and Nodet [9] on the Burgers equation. In the context of Luenberger observer, Boulanger at al. [13] worked on nonlinear hyperbolic conservation laws admitting a linear kinetic formulation which brings us back to the linear case. We can also cite [14], in which the authors design asymptotic observers for discrete-time nonlinear systems and prove their convergence [14]. In addition, several successful applications of the BFN assimilation technique have shown in practice the convergence of this method for nonlinear problems [7, 36] and this motivates our study to develop theoretical tools for nonlinear problems assimilating incomplete data. The BFN has also been used to interpolate altimetric data on a quasi-geostrophic model [28].

The first purpose of this paper is to study the convergence of BFN with the multi-layer quasi-geostrophic (MQG) dynamics commonly used to simulate the mid-latitude ocean circulation. We propose a proof of convergence based on Lyapunov theory. A Lyapunov function is constructed using physical considerations of energy decay that lead to asymptotic convergence. This function must be identical for forward and backward equations in order to ensure continuity and, by the iterative aspect of BFN method, to lead to the initial state convergence. Because observations are not available at every layer of the model, we cannot construct a *strict* Lyapunov function, meaning that the time derivative of the Lyapunov function cannot be found definite-negative but only semi-definite negative. The LaSalle's invariance principle allows us to overcome this problem [11, 22, 25, 26, 27, 40].

The same principle can be used for joint state-parameter estimation when only the prognostic state variable is observed. Finally, and considering realistic observations sampling, the Lyapunov analysis is extended to a partially observed system.

The second main purpose of this paper is to experimentally support our theoretical analysis with numerical experiments. We consider a single-layer quasi-geostrophic ocean model assimilating synthetic altimetric observations mimicking the future Surface Water and Ocean Topography (SWOT; [20, 33]) satellite mission. The SWOT mission, a joint NASA/CNES project with contributions from CSA and UKSA, will be launched in 2022. It will considerably improve the present-day altimetry by providing kilometric-resolution, two-dimensional images of sea surface height (SSH) with a swath wide of 120km and a repeat period of 21 days.

The final purpose is to explore oceanic model improvement by joint state-parameter estimation techniques. The idea is to promote altimetry data, initially designed for state forecasting, to forecast time-varying and hardly observable model parameters. Besides, the inaccuracy of model parameters is a usually neglected aspect that explains some limits of weather forecasting. Yet, highly sensitive parameters badly parametrized have a real impact on state forecasting even with full and perfect available data, as studied in this paper.

The paper is organized as follows. In Section 2, we describe the BFN method applied to the MQG model and partial ocean surface data. A theorem on data assimilation asymptotic convergence is presented in Section 3 for the state estimation. Then, in Section 4, we consider the problem of a joint state-parameter estimation, and we give a framework for the convergence of the BFN algorithm. In Section 5, BFN is used to assimilate synthetic SWOT observations into a quasi-geostrophic model of the ocean circulation in the Gulf Stream region. Our objective is to reconstruct daily maps of the stream function (proportional to SSH) over a period of 21 days. An application to joint state and celerity parameter reconstruction is also presented, associated with a theoretical convergence proof. In Section 6 we draw conclusions.

2. Data assimilation method.

The ocean is a stratified fluid that can be approximately depicted by a stack of layers $k \in \{1, \dots, N\}$ of uniform densities ρ_k with a depth at rest of h_k. The quasi-geostrophic model is a first-order approximation of the Navier-Stokes equations with respect to the Rossby number [34]. The prognostic equation at layer k is:

$$\frac{\partial q_k}{\partial t} + J(\psi_k, q_k) = F_k + D_k, \tag{1}$$

with the following notations :

- ψ_k is the stream function at layer k,
- q_k is the potential vorticity corresponding to the sum of the dynamical vorticity, the thermal (or stretching) vorticity and the planetary vorticity expressed as

$$q_k = \underbrace{\Delta\psi_k}_{dynamical} + \underbrace{(M\psi)_k}_{thermal} + \underbrace{f_k}_{planetary}, \tag{2}$$

  where M is a tri-diagonal matrix defining the inter-connection between layers [25] and $f_k = f_0 + \beta_0 y$ is the Coriolis force supposed to vary linearly in the latitude y (β-plane approximation),

- J is the Jacobian operator, a bilinear and skew-symmetric operator defined by
$$J(f,g) = \frac{\partial f}{\partial x}\frac{\partial g}{\partial y} - \frac{\partial f}{\partial y}\frac{\partial g}{\partial x}, \tag{3}$$
- F is the forcing term driving the dynamics of the model, here the wind stress applied to the surface of the ocean only,
- D represents the dissipation terms due to lateral friction and the bottom friction dissipation at the boundaries of the basin.

We assume that there are no incoming or outgoing fluxes at the boundary $\partial\Omega$ of the two-dimensional domain Ω, which is characteristic of land borders. Mathematically speaking, it is described by Dirichlet boundary conditions

$$\psi^*{}_k(t,x,y) = C_k(t), \quad (x,y) \in \partial\Omega, \tag{4}$$

where the constant $C_k(t)$ can be calculated at each time step in order to satisfy the mass conservation condition on the space domain. Finally, $\psi^*{}_k$ is the stream function spectral coefficient associated to ψ_k, using the eigenvector basis of the matrix M [25].

2.1. **Sea surface height data.** We assimilate observations $\mathcal{Y}(t)$ of the sea surface height (SSH) collected by the altimeter over a finite time window $t \in \mathcal{T} = [t_0, t_f]$. Given a fixed region, at times t_i and on the satellite track $\omega_i \subset \Omega$ depending on the satellite's motion, the satellite captures information expressed as

$$\mathcal{Y}(t,x,y) = \sum_{i=1}^{N_t} \delta(t-t_i)\mathbb{1}_{\omega_i}(x,y)SSH(t_i,x,y), \tag{5}$$

where $\delta(t)$ is the Dirac function and $\mathbb{1}_\omega(x,y)$ is defined as

$$\mathbb{1}_\omega(x,y) = \begin{cases} 1, & (x,y) \in \omega, \\ 0, & \text{otherwise.} \end{cases}$$

A proportional relation between SSH and the upper layer stream function can be found out [39], given by

$$SSH(x,y,t) = \frac{f_0}{g}\psi_1(t,x,y).$$

2.2. **Back-and-forth nudging method.** The standard forward nudging method is an asymptotic observer method forcing the model towards observations, by adding a correction term proportional to the misfit between the observations and the model state. Only asymptotic estimation is achievable for standard nudging (also called asymptotic observer, because it is asymptotically convergent when time goes to infinity), whereas BFN method provides a state estimation over a finite time interval $[t_0, t_f]$ and consequently an initial state estimation [6, 7].

The forward nudging model associated to the MQG model (1) with the observation (5) is expressed as

$$\frac{\partial \hat{q}_k}{\partial t} + J(\hat{\psi}_k, \hat{q}_k) = F_k + D_k + \lambda(\mathcal{Y}(\hat{\psi}_k) - \mathcal{Y}(\psi_k)), \tag{6}$$

where the nudging gain $\lambda > 0$ controls the weight given to the data-correction term. It may depend on the confidence in the data. The term $\mathcal{Y}(\hat{\psi}_k)$ is the projection of the state estimation on the satellite observation domain at layer k.

The backward nudging model is obtained by incorporating a data correction term of the opposite sign (compared to the forward nudging) to the MQG model in decreasing time from t_f to t_0. By change of variable in time $\pi : t \mapsto t_f + t_0 - t$, the backward nudging model defined on $[t_0, t_f]$ is expressed as

$$\frac{\partial \hat{q}_k^b}{\partial t} - J(\hat{\psi}_k^b, \hat{q}_k^b) = -F_k - D_k + \lambda^b(\mathcal{Y}(\hat{\psi}_k^b) - \mathcal{Y}(\psi_k^b)), \tag{7}$$

where the backward nudging gain λ^b is strictly positive but not necessarily equal to the forward nudging gain λ.

To maintain the continuity during the back-and-forth iterations, the forward model (6) is initialized with the last value (at time t_0) of the backward model integration and conversely, the backward model (6) is initialized with the last value (at time t_f) of the forward model integration.

3. **Theoretical analysis.** We want to show that the total energy, defined as

$$V(t) = \sum_{k=1}^{N} E_k(t) + \sum_{k=1}^{N-1} K_k(t) + \sum_{k=1}^{N-2} P_k(t), \tag{8}$$

decays at each back-and-forth iteration towards zero along the error trajectory between the real and the estimated states. The energy E_k represents the enstrophy at layer k defined as

$$E_k(t) = \frac{h_k}{2} \int_\Omega (\Delta \tilde{\psi}_k)^2 dx,$$

the energy K_k is the first order finite difference between layers of kinetic energy defined as

$$K_k(t) = \nu_{k+1}^2 \left\| \nabla(\tilde{\psi}_{k+1} - \tilde{\psi}_k) \right\|_{L^2(\Omega)}^2,$$

and P_k is the second order finite difference between layers of potential energy defined as

$$P_k(t) = \frac{1}{2} \left\| \nu_{k+2}(\tilde{\psi}_{k+2} - \tilde{\psi}_{k+1}) - \nu_{k+1}(\tilde{\psi}_{k+1} - \tilde{\psi}_k) \right\|_{L^2(\Omega)}^2.$$

where $\nu_{k+1} = \frac{f_0^2}{g_{k+\frac{1}{2}}}$, with $g_{k+\frac{1}{2}}$, the so-called *reduced gravity*, expressed as

$$g_{k+\frac{1}{2}} = g_0 \frac{\rho_{k+1} - \rho_k}{\rho_0},$$

with g_0 the average constant of gravity and ρ_0 the average fluid density in the basin Ω. Finally, $\tilde{\psi}_k = \hat{\psi}_k - \psi_k$ is the difference between the real (MQG) and estimated (BFN) stream functions, respectively solutions of (1), and (6)-(7).

Nonlinearities are usually an obstacle for convergence proof. Working on the linearized model is a way to get around it, but higher order information is lost. In this paper nonlinearities of the model will be left unchanged and Lyapunov analysis on V, defined by (8), is particularly suitable for nonlinear equations. An important issue is the unavailability of measurements at deeper ocean levels while our goal is to obtain the convergence at every layer. In such a case the LaSalle's invariance principle, also known as Krasovskii-LaSalle principle, will be used. More specifically, because data are not available continuously in time, we will use the discrete time version of LaSalle's invariance principle, as reminded in the following theorem. Note that V is implictly defined as a function of the stream function ψ [27].

Lemma 3.1 (Barbalat's Lemma). *Let $\mathcal{X} = L^2(\mathcal{T}; H_0^3(\Omega) \cap L^\infty(\Omega))$. Let $V : \mathcal{T} \times \mathcal{X} \to \mathbb{R}$ be a continuously differentiable function such that $\lim_{t\to+\infty} V(t) = \alpha$ with $\alpha < +\infty$. If $\dot{V}$ is uniformly continuous then $\lim_{t\to+\infty} \dot{V}(t) = 0$.*

Theorem 3.2 (Time-discrete LaSalle's invariance principle). *Let $\psi = 0 \in \mathcal{X}$ be an equilibrium and $V : \mathcal{T} \times \mathcal{X} \to \mathbb{R}^+$ be a continuously differentiable function such that*

- *V is positive definite :*
$$\alpha_1(\psi(t)) \leq V(t, \psi(t)) \leq \alpha_2(\psi(t)), \quad t \in \mathcal{T},$$
where α_1, α_2 are functions of class $\mathcal{K}_\infty(\mathcal{X})$[1],
- *ΔV is semi-negative definite with a period of $\epsilon > 0$:*
$$\Delta V(t, \psi(t)) = V(t) - V(t - \epsilon) \leq 0, \quad t \in \mathcal{T},$$
- *V is uniformly continuous;*

then the equilibrium $\psi = 0$ is globally asymptotically stable.

Assumption 1. *Assume there exists a constant $\epsilon > 0$ such that the MQG model associated to the observation (5) is backwardly observable on $[t - \epsilon, t]$ for all $t \in \mathcal{T}$, meaning that there exists a constant $\gamma > 0$ such that*

$$\sum_{k=1}^{N} \int_{t-\epsilon}^{t} \|\mathcal{Y}_k(s, x, y)\|_{\mathcal{X}}^2 ds \geq \gamma \|\psi_1(t, x, y)\|_{\mathcal{X}}^2.$$

Assumption 2. *Assume the stream function belongs to $\mathcal{X} = L^2(\mathcal{T}; H_0^3(\Omega) \cap L^\infty(\Omega))$, $\psi_k \frac{\partial q_k}{\partial y}$ is continuous with regards to y and $\psi_k \frac{\partial q_k}{\partial x}$ is continuous with regards to x.*

Theorem 3.3. *Under Assumptions 1-2, the total energy defined as (8) decays along the back-and-forth error trajectory such that $\tilde{\psi}_k = \hat{\psi}_k - \psi_k$ and $\tilde{\psi}_k^b = \hat{\psi}_k^b - \psi_k^b$ are both global asymptotically stable equilibria.*

See Appendix for the proof of this result.

4. **Joint state-parameter estimation.** An inaccurate representation of model parameters contributes to the model error, and then to the growth of the solution error when time evolves. It therefore affects the ability of our model to accurately fit the observations, and also to predict the evolution of the true state. In the context of geophysical science, most models are either chaotic or highly sensitive to several parameters, which strongly affect long term forecasting results. Some model parameters can be determined only indirectly through classical altimeter data. By sensitivity analysis [15], a technical tool providing the response of a selected function to a certain perturbation, we can evaluate the response of altimeter data to parameter perturbation in order to select the most impacting parameter to be estimated in priority.

State-parameter estimation is based on an augmented state assumption, first introduced by Jazwinski in [24]. The state space is augmented by adding parameters to the control vector to be identified, thanks to data assimilation, so that similar data assimilation techniques developed for state estimation can also be used to parameter estimation. It then assumes that the parameter dynamic is known, which is the case for constant (in time) parameters, but less suitable for unpredictable parameters (e.g. additional model noise that is not governed by deterministic dynamics). Even if it is a well-known research area for standard data assimilation

[1] the functions of class $\mathcal{K}_\infty$ are continuous, strictly increasing, unbounded, vanishing at zero

methods, very few research has been made on state-parameter estimation with nudging data assimilation method. We can nevertheless cite the recent work of Afri [1] addressing semi-nonlinear ODEs (i.e. state model is linear but augmented state model is nonlinear) with standard nudging.

Nudging method can be a very practical method for state-augmentation method. Other data assimilation methods usually require the covariance matrix of error on the background parameter, which can be difficult to determine. This problem is usually overcome with ensemble techniques [29, 30]. For nudging method it is even more simple, as the covariance matrix is unnecessary and replaced by a deterministic gain matrix. Besides, the low computational cost of nudging methods can be very useful in a context where the dimension of the (joint state-parameter) space has been increased.

For the sake of simplicity, let us consider here a one-layer, quasi-geostrophic ocean model ($N = 1$), describing the dynamics of the first baroclinic mode of a flow:

$$\frac{\partial q}{\partial t} + J(\psi, q) = 0, \tag{9}$$

where the potential vorticity q is proportional to the first eigenmode of the Sturm-Liouville equation (see e.g. [2]). Then Equation 2 becomes:

$$q = \Delta\psi - \frac{1}{L_R^2}\psi + f, \tag{10}$$

with L_R the first Rossby radius of deformation [39], and f the Coriolis parameter.

The model parameter to be estimated is the barotropic deformation wavenumber

$$\kappa = \frac{1}{L_R^2} = \frac{f^2}{c^2} \tag{11}$$

where c is the phase speed and $f = 2\Omega\sin(\nu)$ is the Coriolis parameter at latitude ν for the Earth rotation rate Ω (Chelton at al. [16]). This parameter being time independent, it can be seen as a time function solution of

$$\frac{\partial \kappa}{\partial t} = 0. \tag{12}$$

The augmented model is then:

$$\begin{cases} \dfrac{\partial q}{\partial t} + J(\psi, q) = 0, \\ q = (\Delta - \kappa)\psi + f, \\ \dfrac{\partial \kappa}{\partial t} = 0. \end{cases} \tag{13}$$

For the theoretical study and the design of the feedback term, we consider here the ideal case where the observation operator is the identity operator, i.e. $y(t, x, y) = \frac{f_0}{g}\psi(t, x, y)$ for all $t \in \mathcal{T}$ and $(x, y) \in \Omega$ (complete observations). In this case, we propose the following state-parameter nudging (Luenberger) observer. Let $\hat{\kappa}$ be the estimated parameter, and $(\hat{\psi}, \hat{q})$ the estimated state, governed by the simultaneous

state-parameter BFN formulated as follows

$$\begin{cases} \dfrac{\partial \hat{q}}{\partial t} + J(\hat{\psi}, \hat{q}) = \lambda(\hat{\psi} - \psi), \\ \hat{q} = (\Delta - \kappa)\hat{\psi} - \hat{\kappa}\hat{\psi} + f, \\ \dfrac{\partial \hat{\kappa}}{\partial t} = -\dfrac{1}{\alpha}\langle \hat{\psi}, \dfrac{\partial}{\partial t}(\hat{\psi} - \psi)\rangle, \end{cases} \tag{14}$$

where the nudging gains α and λ are strictly positive real numbers to be determined and $\langle \cdot, \cdot \rangle$ is the standard L^2 scalar product on Ω.

The error for the augmented model can then be expressed as

$$\begin{cases} \dfrac{\partial \tilde{q}}{\partial t} + J(\hat{\psi}, \hat{q}) - J(\psi, q) = \lambda\tilde{\psi}, \\ \tilde{q} = (\Delta - \kappa)\tilde{\psi} - \tilde{\kappa}\hat{\psi}, \\ \dfrac{\partial \tilde{\kappa}}{\partial t} = -\dfrac{1}{\alpha}\langle \hat{\psi}, \dfrac{\partial}{\partial t}\tilde{\psi}\rangle, \end{cases} \tag{15}$$

where $\tilde{X} = \hat{X} - X$ for $X = q$, ψ, κ.

Theorem 4.1. *Assume that the stream functions belong to $H_0^1(\Omega)$, then the augmented model error governed by (15) is asymptotically convergent towards zero, associated to a the following positive definite Lyapunov function:*

$$V(t) = \frac{1}{2}\int_\Omega \left\{ |\nabla\tilde{\psi}|^2 + 2\tilde{\kappa}\hat{\psi}\cdot\tilde{\psi} + \kappa|\tilde{\psi}|^2 \right\} + \frac{\alpha}{2}\tilde{\kappa}^2, \tag{16}$$

where the real number $\alpha \in \mathbb{R}_*^+$ satisfies

$$\alpha \geq \frac{1}{\kappa}\sup_{s\geq 0} \|\hat{\psi}(s,x)\|^2_{L^2(\Omega)}. \tag{17}$$

The proof of this theorem is again based on LaSalle's invariance principle. We refer the reader to [2] for a detailed proof.

Remark 1. Note that another Lyapunov function can be found in the one-layer case, expressed as

$$W(t) = \frac{1}{2}\int_\Omega \tilde{q}^2\, dx, \tag{18}$$

representing the error on the potential vorticity.

5. Numerical results.

We now present numerical experiments in order to confirm the theoretical results we obtained in the previous section, and to illustrate the efficiency of the BFN algorithm in the SWOT framework for a multi-layer quasi-geostrophic model. We first look at the numerical schemes used for solving the original MQG (1) and BFN (6)-(7) models.

5.1. Discretization scheme and time-reversibility problems.

Time-reversibility property of the time-discretization scheme represents the ability to preserve the solution after back-and-forth integration without introducing round-off errors. Considering the number of back-and-forth iterations to be performed before reaching convergence, this property is very important for not perturbing the data assimilation process. We can also argue that in many cases time-reversible schemes guarantee the conservation of energy, angular momentum or other quantities.

For this reason, we choose the leap-frog scheme that is a second-order explicit and time-reversible scheme evaluating the same number of functions as the first order

forward-Euler scheme. To prevent the instabilities of the leap-frog scheme caused by the amplitude growth of the computational mode in time, known as *time splitting* [18], we use a Robert-Asselin time filter [4, 35]. Thus, the time-discretization of the MQG model (1) with this scheme reads

$$q_k^{n+1} = \bar{q}_k^{n-1} + 2\Delta t \left(-J(\psi_k^n, q_k^n) + F_k^n + D_k^{n-1}\right),$$

with

$$\bar{q}_k^n = q_k^n + \mu(q_k^{n+1} - 2q_k^n + \bar{q}_k^{n-1}),$$

where $\mu = 0$ refers to the standard leap-frog scheme. In our case, we will choose $\mu = 0.2$ [37].

For spatial discretization, the two-dimensional rectangular domain Ω is divided into a uniform grid and the finite difference (FD) method is applied. It has been observed by Phillips [12] that the FD method applied to the discretization of the Jacobian operator leads to instabilities, not coming from poor choice of boundary condition or coarse space grid, but as an inherent feature of the scheme called *aliasing*. As an alternative, Arakawa [3] has proposed a stable discrete Jacobian that conserves kinetic energy, enstrophy and average wave number. The elliptic equation (2) is discretized with a second-order centered FD scheme.

The dissipative terms D_k make the backward model ill-posed which is very problematic for the use of back-and-forth data assimilation method. In ocean dynamics the dissipation terms are very small compared to the other terms in the model equation (such as wind stress, for example) but cannot be totally neglected. These dissipation terms are mainly designed to take into account subscale phenomena. So, here, this numerical problem is addressed with the diffusive-BFN (DBFN) method [8], that changes the sign of the diffusive terms of the backward model, in order to still account for subscale phenomena in a similar way as in the forward model.

5.2. **Simulation framework.** The reference solution to be retrieved by data assimilation is the solution of the quasi-geostrophic model initialized with an output from the MITgcm [32] Ocean General Circulation Model (OGCM) that simulates the 3D dynamics of the ocean. This model output, shown on Figure 2(a), was distributed along with the SWOT simulator in the first versions of the tool.

The SWOT data are simulated from the reference solution using version 1 of the SWOT simulator. The SWOT simulator [21] is an open-source software developed by NASA and written in Python. From gridded, model fields of SSH, the SWOT simulator generates the SWOT observations grid based on the satellite orbit, interpolates SSH values from the model grid to the SWOT grid, then generates and adds measurement noise consistent with the expected error budget of the satellite [19]. These errors are quantified from numerical simulations of the satellite platform and instrument carried out by the mission project team, and include instrumental errors and geophysical errors due to the presence of water vapor in the troposphere. Note that this error budget has sometimes been modified, and will probably be again modified until the actual use of SWOT satellite, but this should not deeply affect the conclusions of the current study. In the rest of the paper these data with the corresponding errors will be called noisy data.

Consistently with the initial model input, our study is restricted to a spatial domain Ω of size 3099×2052 km covering the highly dynamical Gulf Stream region in the North-Atlantic ocean, divided into a uniform grid of 18 km resolution composed of 170×113 nodes. The time window, into which a state estimate is provided daily, has a length of 21 days, equal to the revisit period of the satellite. After 21 days,

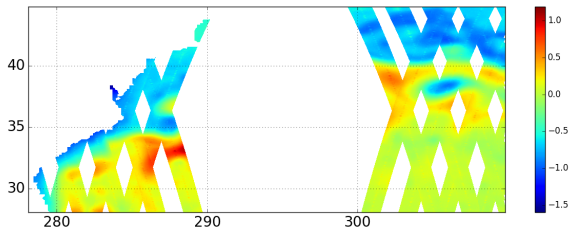

(A) after 5 days

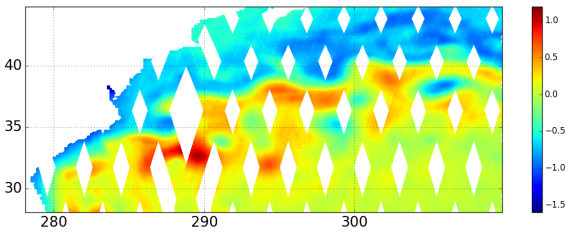

(B) after 10 days

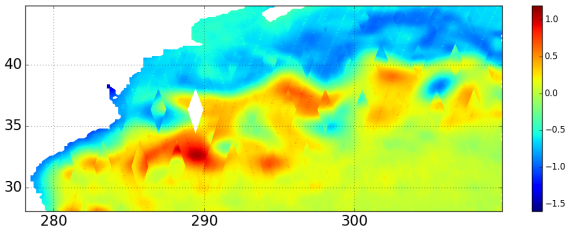

(C) after 21 days

FIGURE 1. SWOT satellite SSH data coverage after 5 days, 10 days or 21 days.

we consider that the coverage of the zone (see Figure 1) is sufficient to satisfy the observability conditions of Assumption 1. The time step is $\Delta t = 600s$, a model integration of 21 days requires then $N_t = 3024$ steps.

To initialize the data assimilation process, the background state comes from the quasi-geostrophic model integrated 10,000 time steps starting from the reference initial state, what we consider to be a sufficiently large number to make the background state distinct from the initial state to be estimated (see Figure 2(b)). As in [25], the wind force is approximated by a steady zonal wind expressed as

$$F(x, y) = -\tau \sin\left(\frac{2\pi y}{L}\right),$$

where y represents the latitude and $L = 3099$ km is the characteristic length of the basin. During the assimilation process over a 21 days time period, we fix $\tau = 0$, thus no external force is applied in our simulations, the nudging term added to the model will play the role of a driving force.

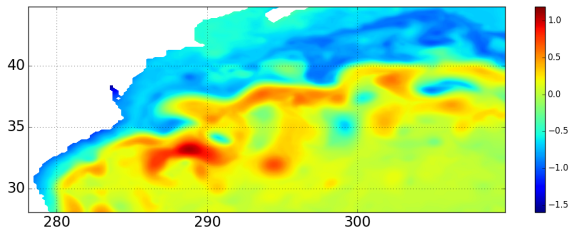

(A) Reference SSH

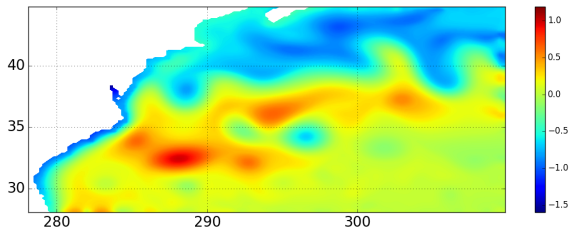

(B) Background SSH

FIGURE 2. Comparison of initial time sea-surface height.

5.3. **Data assimilation parameters.** Observations are only available at certain discrete times, creating discontinuities in the data correction term and as a result in the assimilated state. Nothing indicates in our theoretical results that data frequency has an impact on the asymptotic convergence. Indeed, no matter the amount of data gathered inside the time window, the asymptotic convergence towards the exact solution is theoretically ensured. In practice though, due to the discretization, round-off errors, and non-reversibility, the asymptotic convergence does not necessarily lead to the exact solution.

To measure the influence of data frequency in the data assimilation results, two different frequencies will be tested numerically: one SSH snapshot per 10 time steps and one SSH snapshot per 150 time steps. The last case approximately represents one observation per day for a data acquisition of 21 days. As confirmed by Figure 3, the convergence rate does not seem to be impacted by data frequency. To reduce the discontinuities arising in case of sparse data, we use a mollifier with a compact support of size σ that spreads data around observation times. This mollifier, called bump function, is defined by:

$$\psi_\sigma(s) = \begin{cases} \exp\left(\dfrac{-1}{\left(\frac{\sigma}{2}\right)^2 - |s|^2}\right) & \text{if } |s| < \dfrac{\sigma}{2} \\ 0 & \text{if } |s| \geq \dfrac{\sigma}{2} \end{cases}$$

which is infinitely differentiable, has a compact support of size σ and finally has an integral equal to one after normalization

$$\varphi_\sigma(s) = \frac{\psi_\sigma(s)}{\int_{-\frac{\sigma}{2}}^{\frac{\sigma}{2}} \psi_\sigma(t)dt},$$

with its integral calculated numerically. It can be proven that spreading data at observation times introduces a bias in the error convergence evaluated as

$$\dot{V}(t) \leq h_1 \frac{\lambda f_0}{2g} \sum_{i=1}^{N_t} \varphi_\sigma(t-t_i) \left(-\int_{\omega_i} \tilde{\psi}_1(t)^2 dx + \sigma \sup_{s\in\mathbb{R}^+} \int_\Omega |\partial_t \tilde{\psi}_1(s)|^2 dx \right),$$

where the Lyapunov function increases proportionally to σ. In order to spread data in such a way that we always assimilate at most one observation at a time, the size of the compact support σ_i around the i^{th} observation is calculated as follows

$$\sigma_i = 2\min(t_{i+1} - t_i, t_i - t_{i-1}),$$

where t_j is the mean time where the j^{th} observation is captured in the region. In practice, this choice of compact support ideally balances the effects of smoothing and decorrelation of data to state in time.

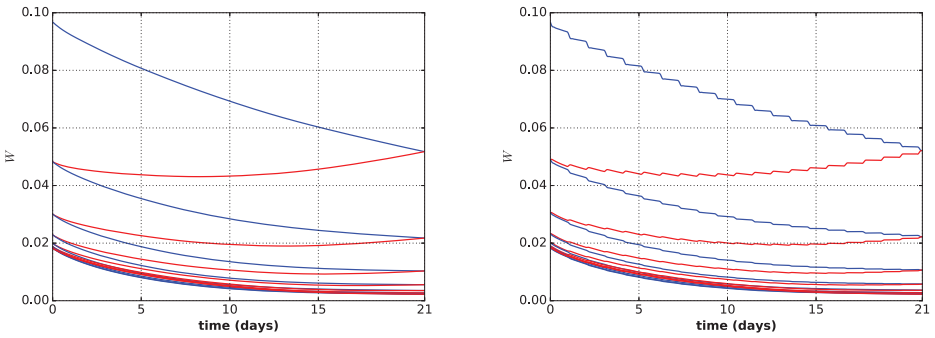

(A) Frequency of $\frac{1}{10}$ (B) Frequency of $\frac{1}{150}$

FIGURE 3. Lyapunov function versus time, during 10 back-and-forth successive iterations (forward integrations in blue, backward integrations in red), while assimilating time-sampled and space-complete data: one observation every 10 time steps (left) and every 150 time steps (right).

The nudging gains are fixed to $\lambda = \lambda^b = 1e^{-16}$ in our experiments. Theoretically, the higher these coefficients, the faster the convergence. In practice, the data collected should not always be trusted due to instrumental errors and enforcing convergence towards these data may lead to poor or non-physical state estimates. Also, high feedback gains amplify the effects previously described due to numerical shocks between observed and non-observed times. Moreover, using small nudging gains allows the model to smooth data along the back and forth iterations (see e.g. [8]). The value $1e^{-16}$ has been selected after analyzing a range of gain values for one iteration of BFN.

The BFN time window is fixed to 21 days, i.e. the revisit period of SWOT. This is theoretically the best choice with respect to observability, since it is the shortest period within which all possibly observed locations are actually observed at least once. Longer time windows may be detrimental to the backward model integrations.

Data type	Error decay at t_0	Error decay at t_f	Error decay in average
Complete data	97.39%	99.99%	99.41%
Time-sampled complete data	88.58%	99.63 %	96.71%
SWOT-like perfect data	77.77%	95.52 %	91.20%
SWOT-like noisy data	77.29%	95.34 %	90.96%

TABLE 1. Percentage of error decay at initial time ($t_0 = 0$ day), at final time ($t_f = 21$ days) and in average over time on $[t_0, t_f]$ after 10 iterations of BFN for different types of data.

5.4. **State estimation.** To validate the theoretical analysis of convergence developed in previous sections, three different scenarios will be experimented: (i) full, perfect (i.e. noise-free) and time-sampled (one data per day) altimetric observations considered as a benchmark with respect to which we measure the performance and the success of other datasets, (ii) perfect SWOT data, and (iii) noisy SWOT data with realistic instrumental and geophysical perturbations.

Figure 4 shows that in all three scenarios, the Lyapunov function is decreasing rapidly during the first BFN iterations, until stabilization around a solution. For full and perfect data, only two iterations are necessary to reach this plateau and for SWOT-like data around ten iterations are necessary. These small numbers of iterations combined with the algorithm simplicity lead to little CPU computing times. For time-sampled complete data in space, the Lyapunov function has been significantly decreased by 96.71% on average over time after 10 iterations of back-and-forth nudging. In comparison, we measure that the Lyapunov function has been decreased by 91.20% for SWOT-like perfect data and 90.96% for SWOT-like noisy data. These results suggest that convergence is very satisfactory considering the sparsity of data. We also note that noise does not have a high impact (see Table 1 for more details). As shown in Figure 4, there is an accumulation phenomenon for the last iterations, and after reaching this plateau, increasing the number of iterations does not improve the final result, the algorithm almost already converged. For instance after 20 iterations the average error decay using SWOT-like data is of 90.71% when after 10 iterations it is of 90.96%, meaning that the final solution did not significantly change during the 10 additional iterations.

We observe in Figure 4 (and also in Figure 3) that the error is not constant over the time window. The error is generally larger at the initial time t_0 than at the final time t_f, and at convergence, it is globally decreasing with time (or increasing with backward time). In the case of full and perfect data, as expected from theoretical analysis, the error is almost equal to 0 at the final time (error decay of 99.99%), but this is not exactly the case at the initial time (error decay of *only* 97.39%). Backward integrations (from t_f to t_0) indeed tend to make the error increase, leading to a slightly degraded estimation of the initial state, compared with the final one. Previous experiments on the BFN algorithm have shown similar behaviours, but it has also been shown (see e.g. [5]) that the estimated initial state, even if it has a larger error, will lead to an as accurate forecast as the estimated final state, the initial error being concentrated along the stable modes of the forward model. So that the estimated final state can be used to forecast in the future ($t > t_f$); and the estimated initial state can also be used to forecast, starting from $t = t_0$.

Figure 5 shows the reference SSH solution and the SSH reconstructed by BFN in the three observational scenarios, for both the initial time t_0 and the final time

t_f. Figure 6 shows the associated errors in the three scenarios, i.e. the differences between the reconstructed SSH and the reference solution.

Overall, and in all scenarios, BFN provides a fair, though not perfect, reconstruction of SSH, particularly at the end of the time window. As it can be expected and is confirmed in Table 1, the reconstruction is better (the residual errors are smaller) in the first, full-observation scenario. The noise in the SWOT observations does not seem to drastically affect the quality of the reconstruction. The reasons behind the non-perfect fit of the BFN solutions to the reference simulation are numerous: the dynamics are not reversible in time when diffusion is included; round-off errors are present; the mollifier plays as if extra, imperfect observations were introduced; the reference simulation is initialized from an OGCM, which physics are poorly represented by a quasi-geostrophic model.

In all scenarios again, the estimation of the state at initial time is less accurate than at final time, as we have seen it on Figure 4, where the Lyapunov function tends to grow during the backward model integration.

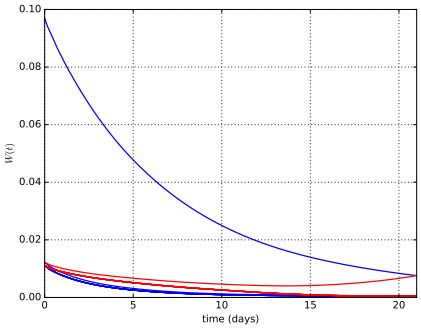

(A) Full and perfect data

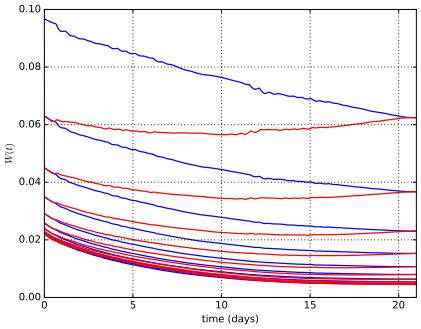

(B) SWOT-like perfect data

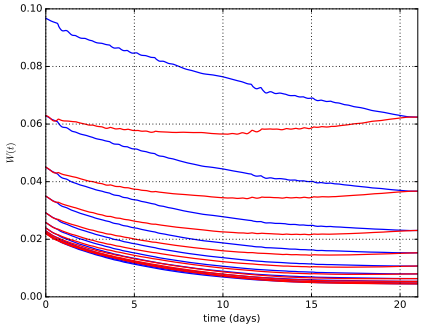

(C) SWOT-like noisy data

FIGURE 4. Lyapunov function during 10 back-and-forth successive iterations (forward integration in blue and backward integration in red) while assimilating different sets of data.

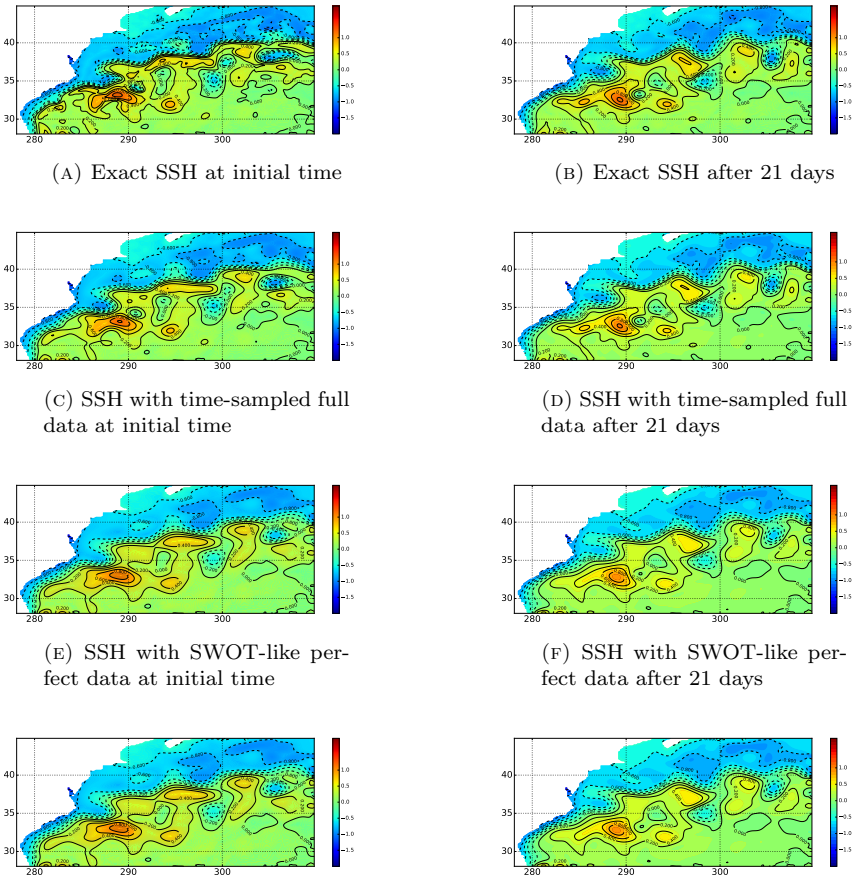

(A) Exact SSH at initial time

(B) Exact SSH after 21 days

(C) SSH with time-sampled full data at initial time

(D) SSH with time-sampled full data after 21 days

(E) SSH with SWOT-like perfect data at initial time

(F) SSH with SWOT-like perfect data after 21 days

(G) SSH with SWOT-like noisy data at initial time

(H) SSH with SWOT-like noisy data after 21 days

FIGURE 5. Sea-Surface Height (exact or assimilated by BFN) in the spatial region Ω at different times : t=0 (first column) and t=21 days (second column).

5.5. **Joint state-parameter estimation.** We study here not only the data assimilation process (time window from 0 to 21 days) but also the impact of the possibly wrong parameter value on the forecast (time window from 21 to 84 days). We only consider here the case of noisy SWOT-like data, and we consider ten iterations of BFN on the time window $[0, 21]$ days.

Three scenarios are investigated: (i) the model uses the true value of the phase speed, $c = 2.5$ (value used for the reference simulation); (ii) the model uses a spurious value $c = 1.0$ that is not corrected by the *standard* BFN assimilation (only state correction); and (iii) the model starts with a spurious value $c = 1.0$ that is corrected among the variables by the joint state-parameter BFN assimilation. Note that the phase speed is the only parameter that could be estimated in this system. Even if we do not drastically change the dynamic regime by slightly modifying the parameter, it is a relatively sensitive parameter of the model.

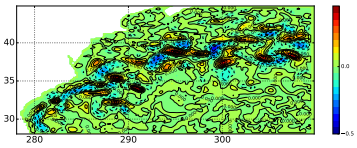

(A) SSH error with time-sampled full data at initial time

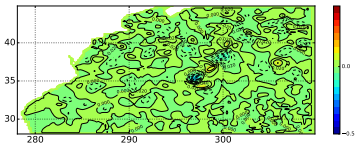

(B) SSH error with time-sampled full data after 21 days

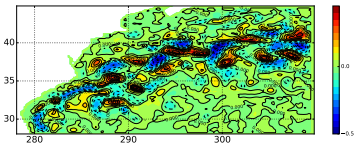

(C) SSH error with SWOT-like perfect data at initial time

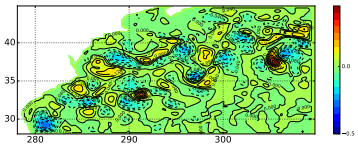

(D) SSH error with SWOT-like perfect data after 21 days

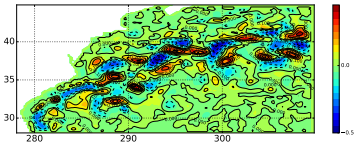

(E) SSH error with SWOT-like noisy data at initial time

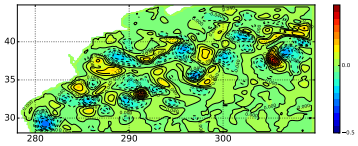

(F) SSH error with SWOT-like noisy data after 21 days

FIGURE 6. Sea-Surface Height spatial error between assimilated and exact maps in the spatial region Ω at different times : t=0 (first column) and t=21 days (second column).

Figure 7 illustrates the results of the three experiments described right above. The first three plots (a-b-c) present the time evolution of the Lyapunov function V (see Equation 16) over the BFN time window and the forecast window. The last plot (d) shows the evolution of the Lyapunov function W (see Equation 18) over the BFN time window.

In the first scenario, as we use the true model parameter, we are in a very similar situation to previous experiments, in the (only) state estimation case. The Lyapunov function, and thus the error on the state, decreases along BFN iterations, and reaches a very small value after several iterations. The error remains small during the forecast period, as the true model parameter is used, and the identified state used for forecasting is almost perfect.

In the second scenario, we use a wrong model parameter, but we assume it is true in the sense that we do not try to correct it. The state estimation process is still efficient, although less than in the first scenario, and the error on the identified state is very small after 10 iterations. But then, using a wrong model parameter quickly leads to a strong increase of the error during the forecast.

In the last scenario, we use a wrong model parameter, but we consider a joint state-parameter estimation, so that the parameter is also corrected during the BFN iterations. The second nudging cœfficient α, for the parameter equation, is fixed according to Equation 17. And as it can be seen on Figure 7-(c), the error on the

state decreases quite quickly and reaches a minimum after less than 10 iterations. And as the parameter is also corrected, the error does not increase much during the forecast period.

Finally, Figure 7-(d) shows the decrease of the Lyapunov function W (see Equation 18) during the assimilation window in the third scenario (joint state-parameter estimation). As $\tilde{\psi}$ decreases to 0 quite quickly (from the decrease of V on figure (c)), the residual in $\tilde{q}$ is then quickly proportional to $\tilde{\kappa}$, the error on the parameter, which is extremely small after 3 iterations. This confirms that the parameter κ is also very efficiently corrected, and the identified parameter is very close to the true parameter. This was expected as the forecast in figure (c) remains very good all along the forecast window.

As a summary, Figure 7 (d) shows that the BFN algorithm extended to joint state-parameter estimation leads to a very accurate identification of the model parameter. The figures (a-b-c) show that the joint state-parameter estimation not only improves the state estimation within the BFN time window, but also during the forecast.

Figure 8 shows the forecasted SSH at 84 days, the end of the forecast window (after 21 days of assimilation and then 63 days of forecast), for the same three scenarios as before: (a) exact speed parameter $c = 2.5$ used for the assimilation and forecast; (b) wrong speed parameter $c = 1.0$ used for the assimilation and forecast; (c) initially wrong speed parameter $c = 1.0$ corrected with data assimilation during the assimilation.

The SSH map in the third scenario is extremely close to the first one, showing again the efficiency of the joint state-parameter identification, as the model parameter has been corrected, allowing the forecast to remain accurate. In the second scenario (wrong and uncorrected model parameter), even if the error on the state is very small after the assimilation window, using a wrong model parameter quickly leads to a poor forecast. The SSH map on figure (b) is indeed far away from the two other maps.

6. **Conclusion.**

The assimilation of large datasets as provided by the future SWOT satellite is a challenging task. Most data assimilation methods currently employed require fine tuning of some control parameters, differentiation of complex state operators or large-scale matrix inversion. In this paper, we have investigated some properties and performance of an alternative method called back-and-forth nudging, a simple and reliable method where none of these tasks are needed. Few studies have been dedicated to testing the assimilation of realistically distributed and big data with back-and-forth nudging.

We first studied the theoretical convergence of the back-and-forth nudging algorithm on the quasi-geostrophic ocean model. We introduced an energy functional, which is actually a Lyapunov function, and proved that it decays with the back-and-forth nudging iterations. We also extended this convergence result to a joint state-parameter estimation problem, where one of the model parameters is not known. Considering another Lyapunov function, we proved that the error (on both state and model parameter) is asymptotically convergent towards zero.

We then carried out numerical experiments to study the actual convergence and efficiency of this algorithm for a quasi-geostrophic ocean model with simulated SWOT data. The major difficulty concerns model time-reversibility, considering

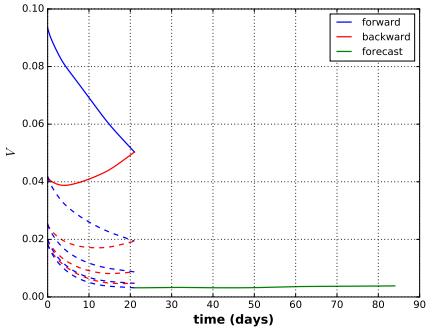

(A) With true parameter $c = 2.5$

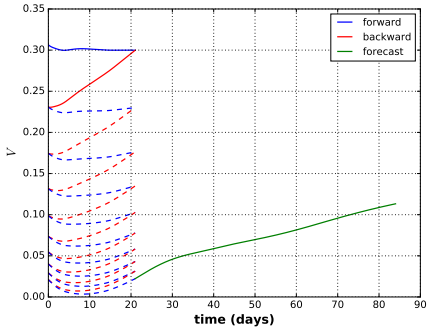

(B) With perturbed parameter $c = 1.0$

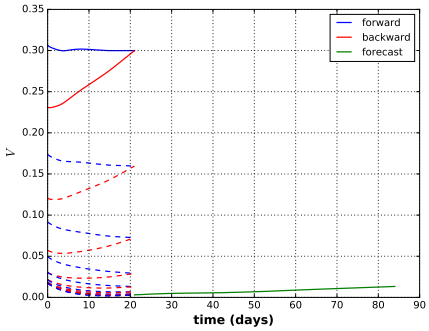

(C) With perturbed parameter $c = 1.0$ and correction

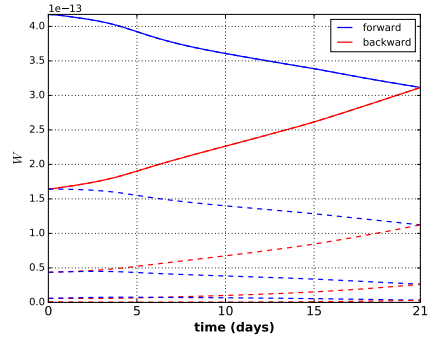

(D) Parameter correction

FIGURE 7. Evolution of the Lyapunov functions V (a-b-c) during the assimilation and forecast windows, and of W (d) during the assimilation window: (a) exact speed parameter $c = 2.5$ used during assimilation and forecast; (b) wrong speed parameter $c = 1.0$ used during assimilation and forecast; (c) initially wrong speed parameter $c = 1.0$ that is corrected during data assimilation; (d) decrease of W during the assimilation window in the third case (c).

the numerous backward integrations in time of this method. The model theoretically needs to be time-reversible, but some specific techniques have been developed if it is not the case. The D-BFN method has been introduced in such a framework, with the idea of changing the sign of the diffusive term in the numerical scheme [8]. But even for time-reversible models, the numerical schemes for time-discretization must conserve the time-reversibility property. The leap-frog scheme is a second-order centered scheme satisfying the time-reversibility requirement, but its tendency to amplify the computational modes can generate severe instabilities. Instead, we have used a filtered leap-frog scheme with a Robert-Asselin filter that guarantees stability, but slightly affects the time-reversibility.

We have seen in our simulations that an empirical determination of the nudging gain (balancing data correction magnitude) is sufficient to obtain convergence in

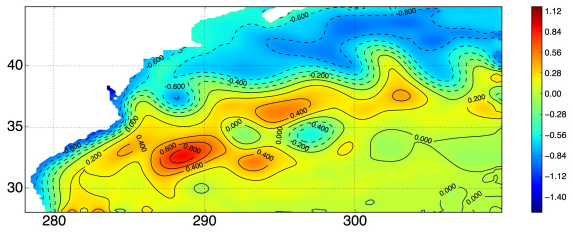

(A) SSH with true parameter $c = 2.5$

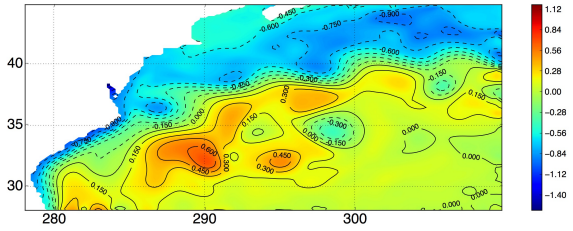

(B) SSH with perturbed parameter $c = 1.0$

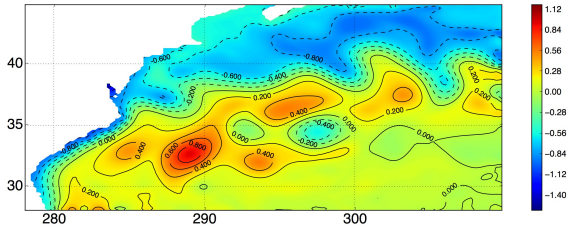

(C) SSH with perturbed and corrected parameter $c = 1.0$

FIGURE 8. Forecasted SSH at 84 days with different scenarios during the full process (data assimilation of 21 days then forecast of 3×21 days): (a) exact speed parameter $c = 2.5$; (b) wrong speed parameter $c = 1.0$; (c) initially wrong speed parameter $c = 1.0$ corrected with data assimilation.

very few iterations. The nudging gain does not need to be optimally determined. In fact, the theoretical analysis we have performed at the continuous level tells us that there are no constraints on the nudging gain to prove convergence, except to be strictly positive for a scalar value and positive definite for a matrix.

Finally, we have seen that the proposed BFN method for a joint state-parameter identification also works in a very similar way. Only few iterations are required to identify both the state and the parameter, so that forecasts are then much more accurate using the corrected parameter.

Additional experiments should be necessary to numerically investigate the observability condition, that may not be completely fulfilled in some cases.

Appendix. In this section, we provide a sketch of the proof of Theorem 3.3. We want to verify if V defined as (8) verifies the three conditions of LaSalle's invariance principle :

- First, we verify that V is a positive definite function with respect to the stream function. Since $\tilde{\psi}_k$ and $\partial_n\tilde{\psi}_k$ vanish at the boundary $\partial\Omega$, by Poincaré's inequality the enstrophy is equivalent to the H^2 norm

$$C_k^1 h_k \|\tilde{\psi}_k\|_{H^2(\Omega)} \leq E_k \leq C_k^2 h_k \|\tilde{\psi}_k\|_{H^2(\Omega)}.$$

  The other terms of V are positive, so V is also equivalent to H^2 norm.
- Second, by noticing that V can be rewritten with the potential vorticity:

$$V(t) = \sum_{k=1}^{N} \frac{h_k}{2} \|\tilde{q}_k\|^2_{L^2(\Omega)},$$

  then the time derivative of V is expressed as

$$\begin{aligned}\dot{V}(t) = &\sum_{k=1}^{N} h_k \int_\Omega \Big(J(\hat{\psi}_k, \hat{q}_k) - J(\psi_k, q_k)\Big)\, \tilde{q}_k dx \\ &- \sum_{i=1}^{N_t} h_1 \lambda \frac{f_0}{g} \delta(t - t_i) \int_{\omega_i} \tilde{\psi}_1 \tilde{q}_1 dx.\end{aligned}$$

  By Green's inequality, $\dot{V}$ satisfies then:

$$\begin{aligned}\dot{V}(t) \leq &\sum_{k=1}^{N} h_k \int_\Omega \Big(J(\tilde{\psi}_k, \hat{q}_k) - J(\psi_k, \tilde{q_k})\Big)\, \tilde{q}_k dx \\ &- \sum_{i=1}^{N_t} h_1 \lambda \frac{f_0}{g} \delta(t - t_i) \|\nabla\tilde{\psi}_1\|^2_{L^2(\omega_i)}.\end{aligned}$$

  From a property of the Jacobian operator $J(\cdot,\cdot)$, for $\psi \in H_0^1(\Omega)$ and $\varphi \in H^1(\Omega)$

$$\int_\Omega J(\psi, \varphi)\psi = 0.$$

  From another property of $J(\cdot,\cdot)$, if there exists two functions $f, g \in C^1(\Omega)$ such that

$$\psi\frac{\partial\varphi}{\partial y} = \frac{\partial f}{\partial y}, \quad \psi\frac{\partial\varphi}{\partial x} = \frac{\partial g}{\partial x},$$

  then we can deduce that

$$\int_\Omega J(\psi, \varphi)\xi \leq 0,$$

  where ψ, φ in $H^1(\Omega)$, $\xi \in L_\infty(\Omega)$. Thus,

$$\begin{aligned}\dot{V}(t) &\leq -h_1 \sum_{i=1}^{N_t} \lambda \frac{f_0}{g} \delta(t - t_i) \|\nabla\tilde{\psi}_1\|^2_{L^2(\omega_i)} \\ &= -h_1 \frac{f_0}{g} \sum_{k=1}^{N} \|\nabla y_k\|^2_{L^2(\Omega)}.\end{aligned}$$

By time integration over $[t-\epsilon, t]$ for all $t \in \mathcal{T}$ and by using the observability assumption 1, we obtain

$$V(t) - V(t-\epsilon) \leq -h_1 \frac{f_0}{g} \int_{t-\epsilon}^{t} \sum_{k=1}^{N} \|\nabla y_k\|^2_{L^2(\Omega)} ds$$
$$\leq -h_1 \gamma \frac{f_0}{g} \|\nabla \tilde{\psi}_1\|^2_{L^2(\Omega)}.$$

which is semi-negative definite.

- Third, let us show that the error stream function trajectory is uniformly continuous. By mutliplication of the error at layer k with $\partial_t \tilde{\psi}_k$, we can show that there exists a strictly positive constant D_k such that

$$\frac{\partial}{\partial t} \|\tilde{\psi}_k\|^2_{H^1(\Omega)} \leq D_k \|\tilde{\psi}_k\|^2_{H^2(\Omega)}. \tag{19}$$

Because $\dot{V}$ is non-increasing and non-negative, the state error $\tilde{\psi}(t)$ is bounded in the H^2 space by

$$\sum_{k=1}^{N} C_k^1 \|\tilde{\psi}_k\|^2_{H^2(\Omega)} \leq V(t) \leq V(t_0).$$

Thus, by the inequality (19), the time derivative of the state $\partial_t \tilde{\psi}(t)$ is bounded in the H^1 space. Meaning that the state trajectory $\tilde{\psi}(t)$ is uniformly continuous in the H^1 space.

Then, by Barbalat's Lemma we can deduce that $\lim_{t\to+\infty} \|\tilde{\psi}_k(t)\|_{H^1(\Omega)} = 0$, which proves the asymptotic stability of the stream function error, and thus proves Theorem 3.3 by considering back and forth iterations as a unique, forward in time, trajectory (using changes of variable on the time variable), and the corresponding time going to infinity when BFN iterations go to infinity.

REFERENCES

[1] C. Afri, V. Andrieu, L. Bako and P. Dufour, State and parameter estimation: A nonlinear Luenberger observer approach, *IEEE Trans. Automat. Control*, **62** (2017), 973–980. https://hal.archives-ouvertes.fr/hal-01232747.

[2] S. Amraoui, *Data Assimilation for External Geophysics: The Back-and-Forth Nudging Method*, PhD thesis, University of Nice Sophia Antipolis, France, 2019.

[3] A. Arakawa, Computational design for long-term numerical integration of the equations of fluid motion: Two-dimensional incompressible flow. Part I, *Journal of Computational Physics*, **1** (1966), 119–143. http://www.sciencedirect.com/science/article/pii/0021999166900155.

[4] R. Asselin, Frequency filter for time integrations, *Monthly Weather Review*, **100** (1972), 487–490.

[5] D. Auroux, P. Bansart and J. Blum, An easy-to-implement and efficient data assimilation method for the identification of the initial condition: The Back and Forth Nudging (BFN) algorithm, in *Proc. Int. Conf. Inverse Problems in Engineering*, vol. 135, J. Phys.: Conf. Ser., 2008.

[6] D. Auroux and J. Blum, Back and forth nudging algorithm for data assimilation problems, *C. R. Math. Acad. Sci. Paris*, **340** (2005), 873–878.

[7] D. Auroux and J. Blum, A nudging-based data assimilation method: the Back and Forth Nudging (BFN) algorithm, *Nonlinear Processes in Geophysics*, **15** (2008), 305–319. https://hal.archives-ouvertes.fr/hal-00331117/document.

[8] D. Auroux, J. Blum and M. Nodet, Diffusive back and forth nudging algorithm for data assimilation, *C. R. Math. Acad. Sci. Paris*, **349** (2011), 849–854.

[9] D. Auroux and M. Nodet, The back and forth nudging algorithm for data assimilation problems: Theoretical results on transport equations, *ESAIM Control Optim. Calc. Var.*, **18** (2012), 318–342.
[10] P. Bernard and V. Andrieu, Luenberger observers for non autonomous nonlinear systems, *IEEE Trans. Automat. Control*, **64** (2019), 270–281.
[11] N. Bof, R. Carli and L. Schenato, Lyapunov theory for discrete time systems, 2018.
[12] B. Bolin, *The atmosphere and the sea in motion: Scientific contributions to the rossby memorial volume*, Rockefeller Univ. Press, 1959.
[13] A.-C. Boulanger, P. Moireau, B. Perthame and J. Sainte-Marie, Data assimilation for hyperbolic conservation laws. A Luenberger observer approach based on a kinetic description, *Commun. Math. Sci.*, **13** (2015), 587 – 622. https://hal.archives-ouvertes.fr/hal-00924559.
[14] L. Brivadis, V. Andrieu and U. Serres, Luenberger observers for discrete-time nonlinear systems, in *2019 IEEE 58th Conference on Decision and Control (CDC)*, Nice, France, 2019, 3435–3440. https://hal.archives-ouvertes.fr/hal-02467958.
[15] W. Castaings, D. Dartus, F.-X. Le Dimet and G.-M. Saulnier, Sensitivity analysis and parameter estimation for distributed hydrological modeling: Potential of variational methods, *Hydrology and Earth System Sciences*, **13** (2009), 503–517.
[16] D. B. Chelton, R. A. deSzoeke, M. G. Schlax, K. El Naggar and N. Siwertz, Geographical variability of the first baroclinic rossby radius of deformation, *Journal of Physical Oceanography*, **28** (1998), 433–460.
[17] A. Donovan, M. Mirrahimi and P. Rouchon, Back and forth nudging for quantum state reconstruction, in *2010 4th International Symposium on Communications, Control and Signal Processing (ISCCSP)*, 2010, 1–5.
[18] D. R. Durran, *Numerical Methods for Wave Equations in Geophysical Fluid Dynamics*, Texts in Applied Mathematics, Springer-Verlag, New York, 1999.
[19] D. Esteban-Fernandez, *Swot Project: Mission Performance and Error Budget*, Technical Report JPL D-79084, NASA/JPL, 2017. https://swot.jpl.nasa.gov/system/documents/files/2178_2178_SWOT_D-79084_v10Y_FINAL_REVA__06082017.pdf.
[20] L.-L. Fu and C. Ubelmann, On the transition from profile altimeter to swath altimeter for observing global ocean surface topography, *J. Atmos. Oceanic Technol.*, **31** (2014), 560–568.
[21] L. Gaultier, C. Ubelmann and L.-L. Fu, The challenge of using future SWOT data for oceanic field reconstruction, *J. Atmos. Oceanic Technol.*, **33** (2016), 119–126.
[22] J.-P. Gauthier and I. Kupka, *Deterministic Observation Theory and Applications*, Cambridge University Press, Cambridge, 2001.
[23] J. E. Hoke and R. A. Anthes, The initialization of numerical models by a dynamic-initialization technique, *Monthly Weather Review*, **104** (1976), 1551–1556.
[24] A. H. Jazwinski, *Stochastic Processes and Filtering Theory*, Courier Corporation, 1970.
[25] E. Kazantsev, Local Lyapunov exponents of the quasi-geostrophic ocean dynamics, *Appl. Math. Comput.*, **104** (1999), 217–257.
[26] N. Kazantzis and C. Kravaris, Nonlinear observer design using Lyapunov's auxiliary theorem, *Systems Control Lett.*, **34** (1998), 241–247.
[27] H. K. Khalil, *Nonlinear Systems; 3rd Ed.*, Prentice-Hall, Upper Saddle River, NJ, 2002.
[28] F. Le Guillou, S. Metref, E. Cosme, C. Ubelmann, M. Ballarotta, J. Verron and J. Le Sommer, Mapping altimetry in the forthcoming SWOT era by back-and-forth nudging a one-layer quasi-geostrophic model, 2020, https://hal.archives-ouvertes.fr/hal-03084218, Preprint.
[29] L. Lei, D. R. Stauffer and A. Deng, A hybrid nudging-ensemble kalman filter approach to data assimilation in wrf/dart, *Quarterly Journal of the Royal Meteorological Society*, **138** (2012), 2066–2078.
[30] A. C. Lorenc, N. E. Bowler, A. M. Clayton, S. R. Pring and D. Fairbairn, Comparison of hybrid-4denvar and hybrid-4dvar data assimilation methods for global NWP, *Monthly Weather Review*, **143** (2014), 212–229.
[31] D. Luenberger, Observers for multivariable systems, *IEEE Transactions on Automatic Control*, **11** (1966), 190–197.
[32] J. Marshall, A. Adcroft, C. Hill, L. Perelman and C. Heisey, A finite-volume, incompressible Navier Stokes model for studies of the ocean on parallel computers, *J. of Geophys. Res.*, **102** (1997), 5753–5766.
[33] R. Morrow, L.-L. Fu, F. Ardhuin, M. Benkiran, B. Chapron, E. Cosme, F. d'Ovidio, J. T. Farrar, S. T. Gille, G. Lapeyre, P.-Y. Le Traon, A. Pascual, A. Ponte, B. Qiu, N. Rascle, C. Ubelmann, J. Wang and E. D. Zaron, Global observations of fine-scale ocean surface

topography with the surface water and ocean topography (SWOT) mission, *Frontiers in Marine Science*, **6**.

[34] J. Pedlosky, *Geophysical Fluid Dynamics*, Springer, 1992.

[35] A. J. Robert, The integration of a low order spectral form of the primitive meteorological equations, *Journal of the Meteorological Society of Japan. Ser. II*, **44** (1966), 237–245.

[36] G. A. Ruggiero, Y. Ourmières, E. Cosme, J. Blum, D. Auroux and J. Verron, Data assimilation experiments using diffusive back-and-forth nudging for the NEMO ocean model, *Nonlinear Processes in Geophysics*, **22** (2015), 233–248. https://hal-amu.archives-ouvertes.fr/hal-01232425/document.

[37] R. E. Schlesinger, L. W. Uccellini and D. R. Johnson, The effects of the Asselin time filter on numerical solutions to the linearized shallow-water wave equations, *Monthly Weather Review*, **111** (1983), 455–467.

[38] D. R. Stauffer and N. L. Seaman, Use of four-dimensional data assimilation in a limited-area mesoscale model. Part I: Experiments with Synoptic-Scale data, *Monthly Weather Review*, **118** (1990), 1250–1277.

[39] C. Ubelmann, P. Klein and L.-L. Fu, Dynamic interpolation of sea surface height and potential applications for future high-resolution altimetry mapping, *Journal of Atmospheric and Oceanic Technology*, **32** (2014), 177–184, http://journals.ametsoc.org/doi/abs/10.1175/JTECH-D-14-00152.1.

[40] B. Zhou, G.-B. Cai and G.-R. Duan, Stabilisation of time-varying linear systems via lyapunov differential equations, *Internat. J. Control*, **86** (2013), 332–347.

Received June 2021; revised February 2022; early access March 2022.

E-mail address: samraoui@groupcls.com
E-mail address: didier.auroux@univ-cotedazur.fr
E-mail address: jacques.blum@univ-cotedazur.fr
E-mail address: emmanuel.cosme@univ-grenoble-alpes.fr